IRIS AperTO

UNIVERSITÀ DEGLI STUDI DI TORINO

AperTO - Archivio Istituzionale Open Access dell'Università di Torino

Transitory and activity-dependent expression of Neurogranin in olfactory bulb tufted cells during mouse postnatal development.

This is the author's manuscript

Original Citation:

Availability:

This version is available http://hdl.handle.net/2318/107513 since 2017-05-18T11:16:01Z

Published version:

DOI:10.1002/cne.23150

Terms of use:

Open Access

Anyone can freely access the full text of works made available as "Open Access". Works made available under a Creative Commons license can be used according to the terms and conditions of said license. Use of all other works requires consent of the right holder (author or publisher) if not exempted from copyright protection by the applicable law.

(Article begins on next page)

25 April 2024

UNIVERSITÀ DEGLI STUDI DI TORINO

***This is an author version of the contribution published on**:*
Questa è la versione dell'autore dell'opera:
[The Journal of Comparative Neurology, 520 (14), 2012, DOI: 10.1002/cne.23150]
ovvero [Gribaudo S., Bovetti S., Friard O., Denorme M., Oboti L., Fasolo A., De Marchis S. 520 (14), Wiley, 2012, pagg.3055-3069]
The definitive version is available at:
La versione definitiva è disponibile alla URL:
[http://onlinelibrary.wiley.com/doi/10.1002/cne.23150/abstract;jsessionid=DA945D1BAD21815004ADF2F5441730B9.f02t02]

Transitory and Activity-Dependent Expression of Neurogranin in Olfactory Bulb Tufted Cells During Mouse Postnatal Development

S. Gribaudo[*], [1] S. Bovetti, [1] O. Friard, [1] M. Denorme[*], [1] L. Oboti[*], [1] A. Fasolo, [1] and De Marchis [1,2 *]
[1]Department of Life Sciences and Systems Biology, University of Turin, 10123 Turin, Italy
[2]Neuroscience Institute Cavalieri Ottolenghi (NICO), 10123 Turin, Italy

ABSTRACT

Neurogranin (Ng) is a brain-specific postsynaptic calmodulin-binding protein involved in synaptic activity-dependent plasticity. In the adult olfactory bulb (OB), Ng is expressed by a large population of GABAergic interneurons in the granule cell layer. We show here that, during postnatal development, Ng is also expressed by OB neurons in the superficial external plexiform layer (sEPL) and glomerular layer (GL). These Ng-positive neurons display morphological and neurochemical features of superficial and external tufted cells. Ng expression in these cells is transient during OB development: few elements express Ng at postnatal day (P) 5, increasing in number and reaching a peak at P10, then progressively decreasing. At P30, Ng is rarely detectable in these neurons. Ng expression in developing tufted cells is also modulated at the cellular level: at earlier stages, Ng labeling is distributed throughout the cell body and dendritic arborization in the GL, but, at P20, when the glomerular circuits are fully matured, Ng becomes restricted to the soma and proximal portion of tufted cell apical dendrites. We show that olfactory deprivation at early postnatal stages induces a strong increase in Ng-positive tufted cells from P10 to P20, whereas no changes have been observed following olfactory deprivation in adult mice. These findings demonstrate that Ng expression in sEPL-GL is restricted to developmental stages and indicate its activity-dependent regulation in a time window critical for glomerular circuit development, suggesting a role for Ng in maturation and dendritic remodeling of tufted cells.

I**NDEXING TERMS:** Ng/RC3; Ca^{2+} ; calmodulin; olfactory deprivation; activity-dependent plasticity

Neurogranin (Ng; also called RC3) is a brain-specific postsynaptic calmodulin (CaM)-binding protein involved in the homeostasis of Ca^{2+} /CaM-mediated signalling (Gerendasy and Sutcliffe, 1997; Gerendasy, 1999; Kubota et al., 2007). Upon binding, Ng regulates the targeting and concentration of Ca^{2+} -free CaM in specific subcellular domains, and it stabilizes CaM, preventing its aberrant activation (Gerendasy and Sutcliffe, 1997; Chakravarthy et al., 1999; Gerendasy, 1999). After a local rise in intracellular Ca^{2+} concentration and phosphorylation by protein kinase C, Ng loses its affinity for CaM, allowing formation of Ca^{2+} /CaM complex and activation of Ca^{2+} /CaM-dependent enzymes (e.g., Ca^{2+} /CaM-dependent protein kinases II and IV, adenylate cyclase, nitric oxide synthase; Gerendasy and Sutcliffe, 1997; Wu et al., 2003). Ng is highly expressed in neurons of the adult brain, including excitatory glutamatergic neurons in the cerebral cortex and hippocampus (Represa et al., 1990; Alvarez-Bolado et al., 1996; Singec et al., 2004) and GABAergic interneurons of the olfactory bulb (OB; Gribaudo et al., 2009). In the mature brain Ng is involved in activity-dependent synaptic potentiation (Pak et al., 2000; van Dalen et al., 2003; Zhabotinsky et al., 2006; Kubota et al., 2007; Zhong et al., 2009, 2011), but studies of postnatal

[*]Present address: Université e Pierre et Marie Curie (UPMC) Paris 6, UMR CNRS 7102, Neurobiologie des Processus Adaptatifs, Paris, France.
[*]Present address: Neuronal and Neuroendocrine Differentiation and Communication Laboratory, INSERM, Sciences Faculty, University of Rouen, France.
[*]Present address: Department of Physiology, School of Medicine University of Saarland, Homburg, Germany.
Grant sponsor: Compagnia di San Paolo, Italy; Grant number: Neurotransplant 2007-0660; Grant number: PRIN 2009; Grant sponsor: Regione Piemonte Azione A (to S.B.); Grant sponsor: LLP/Erasmus Programme between Turin and Rouen Universities (M.D.).
[*]CORRESPONDENCE TO: Silvia De Marchis, Department of Animal and Human Biology, University of Torino, Via Accademia Albertina 13, 10123 Torino, Italy. E-mail: silvia.demarchis@unito.it

hippocampus and cerebral cortex suggested a role for Ng in the maturation of neuronal circuits (Represa et al., 1990; Alvarez-Bolado et al., 1996; Higo et al., 2006). Indeed, Ng expression in these regions peaks in the second or third postnatal week (Represa et al., 1990; Alvarez-Bolado et al., 1996), during a critical period when a burst in synaptogenesis and circuit refinement takes place (Blue and Parnavelas, 1983; Steward and Falk, 1991). In this study, we analyzed the profile of Ng immunoreactivity during OB postnatal ontogenesis.The basal OB circuitry starts to be established between embryonic day (E)11.5 and E15 (Treloar et al., 1999), when the axons of the olfactory sensory neurons (OSNs) reach the presumptive glomerular layer (GL) and contact the apical dendrites of mitral and tufted cells (Blanchart et al., 2008). These cells are the first to be generated in the developing OB in a time window beginning at E11 and lasting until E14 for mitral cells and until late embryonic/perinatal stages for tufted cells (Hinds, 1968; Winpenny et al., 2011). At E14–E15, the presumptive granule cell layer (GCL) and GL start to be populated by GABAergic interneurons (Wichterle et al., 2001). Between P5 and P15, mitral and tufted cells undergo extensive refinement of the immature and broadly spread dendritic arborizations until a single apical dendrite remains, confined to one glomerulus (Frazier and Brunjes, 1988; Treloar et al., 1999; Matsutani and Yamamoto 2000; Lin et al., 2000; Belluscio et al., 2002; Imamura and Greer, 2009). Dendritic remodelling and pruning are accompanied by an increase in the number of synapses between P10 and P15 and can be modulated by olfactory sensory activity (Blanchart et al., 2006; Whitman and Greer, 2007; Imamura and Greer, 2009).
The molecular mechanisms underlying dendritic development of mitral and tufted cells are largely unknown. Here we found that Ng is transiently expressed in subsets of tufted cells in a developmental phase matching with tufted cell morphological maturation and dendritic remodeling, suggesting a role for Ng in these processes. Interestingly, we demonstrated that olfactory deprivation performed in early postnatal life, but not during adult hood, positively regulates Ng expression in these cells, indicating Ng as a possible molecular mediator of a compensatory response that could attenuate the functional consequences of reduced early experience for OB development.

MATERIALS AND METHODS

Animals

Experiments were performed on postnatal day (P) P0–1, P5, P10, P15, P20, P30, and 8-week-old CD1 strain
mice (Charles River, Calco, Italy). All animals were housed under a 12-hour light-dark cycle in an environmentally controlled room. All experimental procedures were in accordance with the European Communities Council Directive of 24 November 1986 (86/609 EEC), Recommendation 18/06/2007, Dir. 2010/63/UE, and the Italian law for care and use of experimental animals (DL116/92) and were approved by the Italian Ministry of Health and the Bioethical Committee of the University of Turin.

Olfactory deprivation

For early postnatal deprivation, newborn mice (P0–P1) were lightly anesthetized by hypothermia, and a small polyethylene plug was introduced into one naris, followed by a brief cauterization of the skin. The pups were quickly revitalized under a heat lamp and subsequently returned to the dam. Naris closure blocks the incoming of airflow in the naris and olfactory stimuli in the unilateral olfactory bulb (Brunjes, 1994). Deprived mice were monitored over the time to assess the persistence of naris occlusion. Mice showing naris reopening were excluded from the study. Control animals did not undergo naris closure. Pups from deprived and control groups were killed at P5, P10, P15, P20, and P30 (at least four animals for each age).
For olfactory deprivation in P30 mice, animals were lightly anesthetized with a solution of ketamine (Ketavet; Gellini, Aprilia, Italy) and xylazine (Rompun; Bayer, Wuppertal, Germany) before inserting the nose plugs (polyethylene tubing, 0.7 mm) into one naris for 10 days (shortterm

deprivation) or 42 days (long-term deprivation; n = 4 for each time; Cummings et al., 1997). The effectiveness of olfactory deprivation was checked by verifying that the nose plug was retrieved in the anterior part of the snout at the end of the experiment and confirming the reduced level of TH expression in the GL of the OB by immunohistochemistry (Baker et al., 1993). Animals from which the plug was not retrieved or that did not show decreased TH expression were discarded.

Zinc sulfate nasal irrigation

Adult (8 weeks old, n = 8) mice received intranasal administration of zinc sulfate (50 µl, 0.17 M; Sigma, St. Louis, MO) to destroy mature and immature OSNs (Ducray et al., 2002; Williams et al., 2004) or 0.9% saline solution as control. Zinc sulfate or saline solution was injected in both naris 10 minutes apart, by a syringe with a blunted, 4-mm-long needle inserted into the naris. After intranasal irrigation, animals were held for several seconds with the head down to minimize spread of the solution to the oral cavity (Giachino et al., 2005). Animals were killed 21 days following irrigation.

Tissue preparation and sectioning

Depending on age, mice were deeply anesthetized by hypothermia (P5) or with an intraperitoneal injection of a mixture of ketamine (Ketavet; Gellini) and xylazine (Rompun; Bayer) and perfused transcardially with 0.9% saline, followed by 4% paraformaldehyde in 0.1 M phosphate buffer (PBS), pH 7.4. Brains were removed from the skull; postfixed for 4–6 hours in the same solution; cryoprotected in a 30% sucrose solution in 0.1 M phosphate buffer, pH 7.4; frozen; and cryostat sectioned (Leica Microsystems, Milan, Italy). Free-floating coronal serial sections 25 lm thick containing the OB were collected in multiwell dishes. Sections were stored at -20° C in antifreeze solution until use.

Immunohistochemistry

Sections were incubated overnight at 4° with primary antibodies diluted in 0.01 M PBS, pH 7.4, and Triton (0.2% for P5, P10, P15 tissues, 0.5% for P20 and P30 tissues) and with 1% normal serum of the same species of the secondary antibody. The primary antibodies used were anti-neurogranin (Ng; 1:1,000; rabbit, polyclonal IgG; Chemicon, Temecula CA; catalog No. AB5620), antiolfactory marker protein (OMP; 1:6,000; goat, polyclonal antibody, IgG; gift from F. Margolis, Baltimore, MD), antityrosine hydroxylase (TH; 1:3,000; mouse, monoclonal antibody, IgG; Immunostar, Hudson, WI), anti-calbindin (CB; 1:3,000; mouse, monoclonal antibody, IgG; Swant; Bellinzona), anti-calretinin (CR; 1:5,000; monoclonal antibody IgG; Swant), anti-glutamic acid decarboxylase 65 (GAD65; 1:1,000; monoclonal antibody, IgG; Developmental Hybridoma Bank, Iowa City, IA), anti-glutamic acid decarboxylase 67 (GAD67; monoclonal antibody, IgG, Chemicon), anti-cholecystokinin (CCK; 1:2,000; rabbit, polyclonal antibody, IgG; a generous gift from Philippe Ciofi, France); anti-T-box transcription factor 21 (Tbx21; 1:10,000; rabbit, polyclonal antibody, IgG; a generous gift from Yohihiro Yoshihara, Japan), and anti-microtubule associated protein 2 (MAP2; 1:1,000; mouse, monoclonal antibody; Chemicon, Millipore, Billerica, MA). Sections were then incubated for 1 hour at room temperature (RT) with secondary antibodies diluted in 0.01 M PBS, pH 7.4. Secondary antibodies used were as follows: anti-mouse, anti-rabbit and anti-goat Cy3-conjugated (1:800; Jackson Immunoresearch, West Grove, PA); anti-mouse, anti-rabbit, and anti-goat 488 (1:400; Alexa Fluor; Molecular Probes, Eugene, OR); or anti-mouse, anti-rabbit, and antigoat biotinylated (1:250; Vector, Burlingame, CA), followed by avidin FITC incubation (1:400; Jackson Immunoresearch). When two polyclonal primary antibodies were used (anti-Ng/anti-Tbx21, anti-Ng/anti-CCK), staining of the first antigen–antibody complex was performed with a goat anti-rabbit Cy3-conjugated (1:800; Jackson Immunoresearch) secondary antibody. This step was followed by 30 minutes of incubation with normal rabbit serum (1:1,500). After rinsing in PBS, slices were incubated with a blocking solution with an anti-rabbit Fab fragment (Jackson

Immunoresearch) for 1 hour (RT), followed by PBS washes and fixation (4% formalin for 20 minutes). After PBS washes, sections were incubated with the second primary antibody, which was visualized by using a goat anti-rabbit biotinylated antibody (1:250; Vector) and avidin FITC (1:400; Jackson Immunoresearch). Sections were counterstained by incubation with the nuclear dye 4,6-diamidino-2-phenylindole (DAPI) for 5 minutes, followed by a wash in PBS, and then mounted onto slides and coverslipped with a 1,4-diazobicyclo-(2,2,2)octane (DABCO)-based antifade mounting medium.

Antibody characterization

See Table 1 for a list of all antibodies used.

The Ng antibody detected on Western blotting a band at the expected molecular weight of 14 kDa, corresponding to Ng, and a slighter band at 43 kDa, corresponding to growth-associated protein 43 (GAP43; Gribaudo et al., 2009). As previously reported, no band corresponding to Ng was detected by immunoblot analysis in tissue extracts obtained from cerebral cortex and hippocampus of Ng knockout mice (Pak et al., 2000). By immunohistochemistry, no staining was observed in any brain regions when the antibody was used in Ng knockout mice (Pak et al., 2000; Larouche et al., 2006). Control for specific immunostaining indicates that Ng antibody does not react with GAP43 on tissue slices (Larouche et al., 2006; Gribaudo et al., 2009). Staining with Ng antiserum was consistent with in situ hybridization for the mRNA of the same protein in cortex and hippocampus (Singec et al., 2004).

The OMP antibody was generated by Dr. Frank Margolis (University of Maryland). It recognized a single band of 19 kDa molecular weight corresponding to OMP on Western blots of mouse and rat olfactory bulb (Baker et al., 1989). It immunolabeled a cell population that had been morphologically classified as mature olfactory neurons in the rodent olfactory neuroepithelium in a number of previous studies (e.g., Verhaagen et al., 1989; Schwob et al., 1992; Kondo et al., 2010).

The Tbx21 antibody was generated by Dr. Yoshihiro Yoshihara (Yoshihara et al., 2005). Tbx21 is specifically expressed in mitral/tufted cells (Faedo et al., 2002), and the antibody showed specific labeling of the mitral/tufted cells in mouse OB by immunofluorescence (Yoshihara et al., 2005). The antibody gave no signal on the OB sections prepared from Tbx21 knockout mice (Mitsui et al., 2011), confirming its specific reactivity to Tbx21 protein.

The CCK-8 antiserum was raised against synthetic porcine nonsulfated, Ct-amidated octapeptide (CCK-8) coupled to bovine thryoglobulin with glutaraldehyde. Characterization by radioimmunoassay showed cross-reactivity with CCK-33 and gastrin but no cross-reactivity with substance P, Leu- or Met-enkephalin, β-endorphin, or FMRFamide (Studler et al., 1984). Immunocytochemical labeling is abolished in rodent brain by preadsorption with 10^{-6} M CCK-8 and gastrin 1, but not by neurotensin, human growth hormone-releasing hormone (GHRH), porcine neuropeptide Y, substance P, or leu- or Met-enkephalin (Ciofi and Tramu, 1990). The distribution of CCK-immunoreactive cell bodies reported here matches the mapping of CCK mRNA expression in mouse brain (Allen Institute Brain Atlas; Porteous et al., 2011).

The CB antibody D28k reacts specifically with calbindin on immunoblots of tissue extracts from human, monkey, guinea pig, rabbit, rat, mouse, and chicken. The antibody does not cross-react with calretinin (CR) or other known calcium-binding proteins and specifically stains the ^{45}Ca binding spot of calbindin D-28k (MW 28,000, IEP 4.8) in a two-dimensional gel. With immunohistochemistry, this anti-body specifically localizes CB on brain sections and does not stain in the brain of calbindin D-28k knockout mice (manufacturer's technical information).

The CR antibody 6B3 recognizes an epitope within the first four EF-hand domains common to both calretinin and calretinin-22k. On Western blot, the anti-calretinin antibody detects a band at the expected molecular weight of 29 kDa in brain extracts. This antibody does not cross-react with calbindin D-28k or other known calcium-binding proteins, as determined by its distribution in the brain as well as by Western blot. No staining was observed in any brain regions when the antibody was used in CR knockout mice (manufacturer's technical information).

The mouse monoclonal TH antibody labels a single band at approximately 62 kD corresponding to TH and does not cross-react with dopamine-β-hydroxylase, dihydropterdine reductase, phenylethanolamine-N-methyl-transferase, phenylalanine hydroxylase, or tryptophan hydroxylase. The antibody has a wide species cross-reactivity. The specificity of the TH antibody has been examined by preabsorption of the antibody with a high concentration of TH (Van Bockstaele and Pickel, 1993). Omission of the primary antibody abolished any detectable immunoreactivity (Reyes et al., 2007).
The GAD67 antibody detects on Western blot a band at the expected molecular weight of 67 kDa and does not-cross react with the GAD65 isoform in rat brain lysate (manufacturer's technical information).
Affinity-purified GAD from adult rat brain was used to raise an anti-GAD65 monoclonal antibody in mouse. Rat GAD65 has 98% amino acid sequence homology to mouse GAD65 (NCBI Blast). The GAD65 antibody detects on Western blot a single band at the molecular weight of 64 kDa in rat brain lysate (manufacturer's technical information). The corresponding band was absent in Western blots of mouse brain tissue taken from a GAD65 null mouse (Yamamoto et al., 2004).

TABLE 1
Primary Antibodies

Antigen	Immunogen	Source, species, catalog No.	Dilution used
Neurogranin (Ng)	Recombinant rat Ng, complete sequence	Chemicon (Millipore, Billerica, MA), rabbit polyclonal, AB5620	1:1,000
Olfactory marker protein (OMP)	Purified rodent OMP	F. Margolis (Univ. Maryland), goat, polyclonal	1:6,000
T-box transcription factor 21 (Tbx21)	Synthetic peptide, 20 aa (GAPSPFDKETEGQFYNYFPN) from C-terminal of mouse	Y. Yoshihara (Saitama, Japan), rabbit, polyclonal	1:10,000
Cholecystokinin (CCK-8)	Synthetic porcine unsulfated CCK-8 (DYMGWMDF-NH2)	P. Ciofi, (Bordeaux, France) rabbit, polyclonal	1:2,000
Calbindin (CB)	CB D-28k purified from chicken gut	Swant (Bellinzona, Switzerland), mouse, monoclonal, 300	1:3,000
Calretinin (CR)	Recombinant human CR-22k	Swant, mouse, monoclonal, 6B3	1:5,000
Tyrosine hydroxylase (TH)	Denatured TH from rat pheochromocytoma	Immunostar (Hudson, WI), mouse, monoclonal, 22941	1:3,000
Glutamic acid decarboxylase 67 (GAD67)	Recombinant GAD67 protein	Chemicon (Millipore), mouse, monoclonal, MAB5406, clone 1G10.2	1:5,000
Glutamic acid decarboxylase 65 (GAD6)	GAD affinity purified from rat brain	Developmental Studies Hybridoma Bank (Univ. Iowa), mouse, monoclonal	1:1,000
Microtubule-associated protein 2 (MAP-2)	Bovine brain microtubule protein	Chemicon (Millipore), mouse, monoclonal, MAB3418	1:1,000

MAP2 antibody localizes the high-molecular-weight forms of MAP2, namely, MAP2a and MAP2b, by Western blot (WB; manufacturer's data sheet). MAP-2 is a stringent marker for neurons. In addition, MAP-2 displays intracellular specificity. In the central nervous system, MAP-2 is confined to neuronal cell bodies and dendrites. There are exceptions, however, in which some axons stain positively for small amounts of MAP-2. MAP-2 is uniformly distributed throughout the cell when first expressed in cultured neurons but becomes selectively localized as dendritic development proceeds (Dotti, 1987).

Cell counting

Cell counts and image analysis were performed on a Nikon microscope coupled with a computer-assisted image analysis system (Neurolucida software; MicroBrightField, Colchester, VT) or on a Fluo-View 500 confocal microscope (Olympus Instruments, San Francisco, CA). Confocal image z-stacks were captured through the thickness of the slice at 1-lm optical steps. These image stacks were used for cell counting or assembled into extended-focus photographs and brightness, color, and contrast balanced and assembled into panels with Corel-Draw 11 (Corel, Ottawa, Ontario, Ontario).
Cells were counted using a systematic random sampling method, applied to three sections per animal, positioned at anterior, medial, and posterior level through the OB. Sampling of the superficial portion of the EPL (sEPL, which includes the high-nuclear-density zone of the EPL just below the GL) and the GL, collectively defined as the sEPL-GL region (see Fig. 2L–P), was performed by applying a virtual counting grid (square's size 80 x 80 μm) onto each section. The sEPL-GL region was delimited by using DAPI staining. Cells were counted through the 25 μm

thickness of the slice in one square of the grid (one of every two) by sequential translation of the counting frame until the area of interest was entirely covered. This procedure allowed us to analyze about one-fourth of the area of interest. The number and position of each cell in the counted area were marked by the software. Cells contacting a line on the upper or left edge of the counting square were excluded from and cells contacting the lower or right edge of the square were included in the counts.
Cell density (number of labeled profiles/mm^2) was calculated, and the total number (T) of labeled cells was estimated by using the formula: $T = (N \times V)/t$, where N is the cell density in the layer, V the volume, and t the thickness of the sections.
To estimate the volume of each layer, drawings of sections (six to eight sections per animal, 150-µm intersection intervals for P5, 200 µm for P10 and P15, 275 µm for P20) through the entire OB (from the anterior MOB to the anterior AOB) were made from low-magnification photographs using Neurolucida software. The boundaries between layers were traced based on DAPI staining. The area of each section and layer in the traces was automatically calculated by Neurolucida software, and the total volume of the OB and layers was estimated applying the Cavalieri method.

Estimation of the size of glomeruli
The size of the glomeruli at the different postnatal stages and following olfactory deprivation was obtained by estimating glomeruli area and diameter following immunostaining for the OMP (Margolis, 1982), which labels mature olfactory sensory neurons, revealing the glomerular axonal compartment (Kasowsky et al., 1999). MAP-2 immunostaining was employed to measure the glomerular dendritic compartment (Kasowsky et al., 1999) at P20 under control and deprived conditions.
Glomeruli area was calculated by applying a virtual counting grid (square's size 20 x 20 µm) onto three sections per animal (anterior, medial, and posterior levels). Every glomerulus was analyzed through the 25-µm thickness of the slice on the entire GL area. For each glomerulus, the number of grid intersections included in the glomerulus area (OMP-positive or MAP-2-positive) was counted and marked by the software. Intersection points contacting the upper or left edge of the glomerulus were excluded and intersection points contacting the lower or right edge of the glomerulus were included in the counts. If only one intersection point was contained in the glomerulus area, its area can be estimated to be 400 μm^2 (20 x 20 µm). Thus, the area of each glomerulus was counted by using the formula: area (A) = (number of points) x 400 μm^2. Assuming that this area is circular, the diameter (d) is obtained from $d = 1.13 \times A(1/2)$. However, according to stereological principles, the measured diameter is smaller than the true diameter. To correct this underestimation, the diameter was multiplied by a correction as follows: true mean diameter $D = (4/\pi) \times d$ (Meisami et al., 1990).

Analysis of cell body size and position
Cell bodies of Ng-expressing cells residing in the sEPL-GL region were drawn on live images (Neurolucida software). Depending on age, analyses were conducted on all Ng-positive cells (P5 and P20) or using a random sampling method by applying a virtual counting grid (square size 80 x 80 µm) onto the section of interest (P10 and P15) as previously described (see above). Three sections positioned at anterior, medial, and posterior levels through the OB from at least two animals for each age were evaluated. In total about 200 cells per age were considered for the analysis. To correlate cell body size with its distance from the sEPL-GL lower border, we developed a software (Neurolucida Companion for Spatial Distribution analysis [NCSD]); available online at the site http://www.personalweb.unito.it/olivier.friard/ncsd. For each cell, NCSD software estimates the area, mean diameter, and corresponding distance from the sEPL-GL lower reference line. During development the thickness of the GL varies with age, so the distance of Ng-positive cells from the lower edge of the sEPL-GL region was normalized by imposing the extension of the sEPL-GL area at different postnatal ages to 100.

Statistical analysis
The normal distribution was assessed by the Kolmogorov-Smirnov test, and statistical comparisons were conducted by univariate ANOVA, followed by Student's *t*- test when appropriate. The distribution of soma size for each group was fitted with one or two Gaussian curves in the software Origin 7J. Significance was established at $P < 0.05$. All cell counts and volumes are presented as mean ± SEM and are derived from at least three different animals for each group and each age unless otherwise indicated.

Photomicrograph production
Images were processed in NIH Image J (http://rsb.info.nih.gov/ij/) and Adobe Photoshop 7.0 (Adobe Systems, San Jose, CA) and assembled into montages in CorelDraw 11. Only general adjustments to color, contrast, and brightness were made.

RESULTS
Ng is transiently expressed in cells of the sEPL-GL region during OB development
Ng expression has been investigated during OB development at different postnatal ages (from P0 to P30; Fig. 1) by immunofluorescence analysis. Starting from P0, Ng identifies a population of granule cells (Gcs) whose immunopositive apical dendrites ramify in the presumptive EPL (not shown). By P20, the deep to superficial gradient of distribution typical of Ng-expressing granule cells in the adult OB (Gribaudo et al., 2009) becomes distinguishable. At P5, mitral cell bodies faintly labeled for Ng can be observed (Fig. 1P). Starting from P5, Ng is also expressed by a population of cells lying in the superficial portion of the EPL or in the GL (herein defined as the sEPL-GL region; Figs. 1, 2L,P). The density of Ng-positive cells in this region increases with age, reaching a peak at P10 and progressively being reduced thereafter (Fig. 1O). Ng-positive cells show a single apical dendrite that arborizes in a complex tuft within single glomeruli and one or few basal processes oriented toward the EPL (Fig. 1Q), where they intermingle with the intense Ng-positive neuropil formed by apical GC dendritic processes (Fig. 1H,M). The extension and intensity of Ng labeling in the apical dendritic tuft increase progressively from P5 to P15, in parallel with glomeruli enlargement (Fig. 1A–I). At P20, concurrently with a reduction in the number of labeled cells, Ng expression becomes mainly restricted to the cell bodies and to the proximal portion of apical dendrites, suggesting a downregulation of the protein in the distal cellular compartment (Fig. 1L–N). At P30, only rare Ng-positive elements are identifiable in the sEPL-GL region (Fig. 1O), a condition that is maintained at adult ages (Gribaudo et al., 2009). Conversely, GCs in the GCL retain Ng throughout life, indicating distinct temporal dynamics in Ng expression between OB projection neurons and interneurons.

Heterogeneous populations of tufted cells express Ng during development
The morphological features of Ng-expressing cells in the sEPL-GL region (e.g., position, dendritic arborization in the GL, lack of spines) are reminiscent of tufted cells (Pinching and Powell, 1971; Macrides and Schneider, 1982; Orona et al., 1984; Antal et al., 2006; Ennis et al., 2007). Moreover, we found that their soma diameter varies from a minimum of 7.6 to a maximum of 15.7 μm (n = 827 total cells analyzed, from two animals for each age, at least 200 cells/age), a range that fits with tufted cell body size (Pinching and Powell, 1971; Kosaka and Kosaka, 2007). To confirm further that Ng-positive elements in the sEPL-GL belong to the tufted cell population, we performed double immunostaining for Ng and Tbx21 or CCK peptide (Fig. 2A–F), two markers of tufted cells (Liu and Shipley, 1994; Faedo et al., 2002; Allen et al., 2007; Mitsui et al., 2011). At P10, when the number of Ng-positive cells in the sEPL-GL reaches its maximum, 47.4% ± 3.2% of Ng-expressing cells are Tbx21-positive (n = 3; mean ± SEM; Figs. 2A–C, 3F), and 40.4% ± 4.5% are CCK-positive (n =4 3; mean ± SEM; Fig. 2D–F). Moreover, double-labeling analysis with markers of periglomerular interneurons shows no colocalization between Ng and CB, CR, or TH (Fig. 2G–I). Coherently, Ng never colocalizes with GAD65/67 (Fig. 2J), the two enzyme isoforms of glutamic

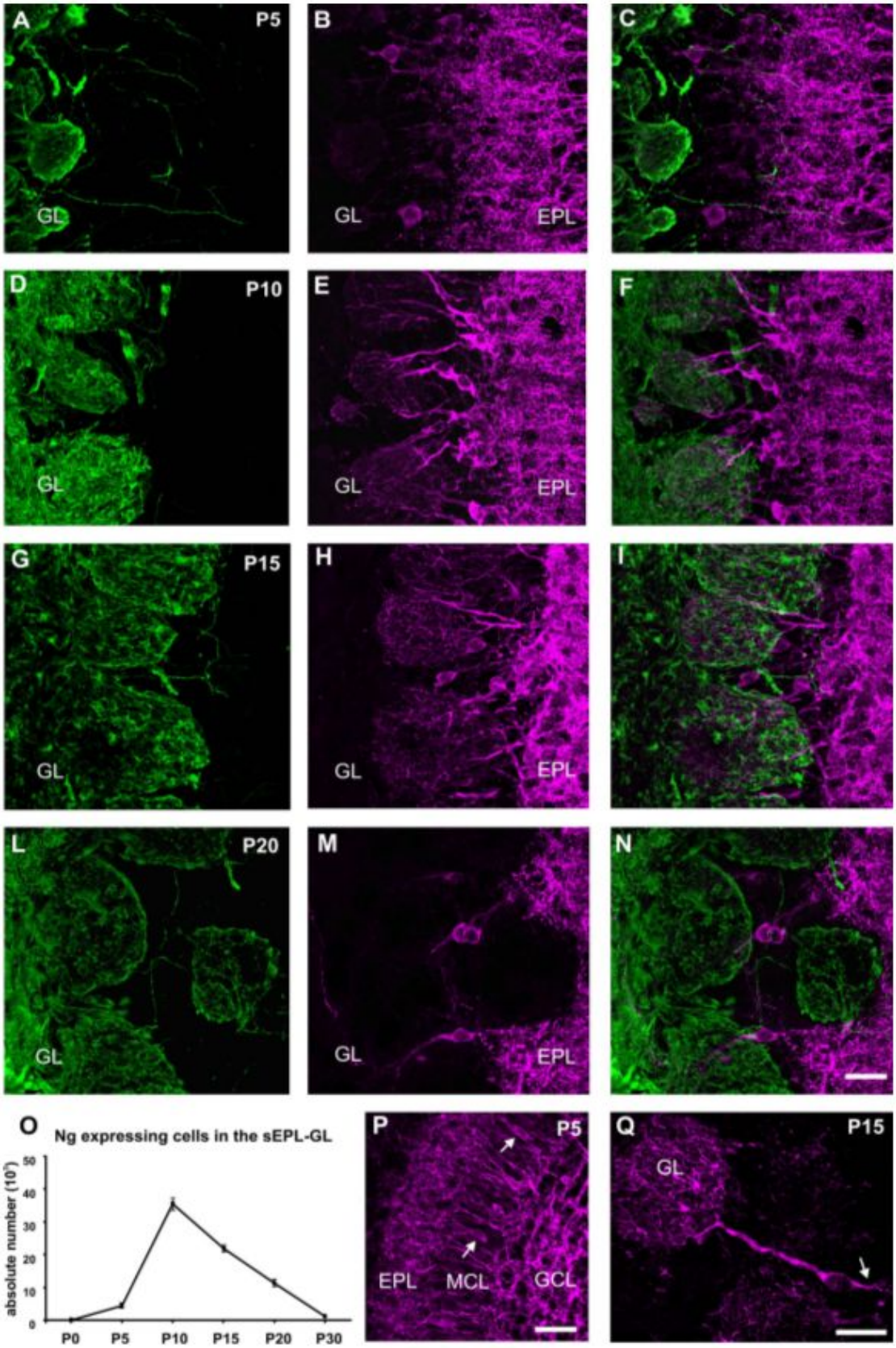

Figure 1. Ng-expressing cells in the sEPL-GL region of the developing OB. A–N: Images of sEPL-GL region at different postnatal ages (P5–P20) stained in green for OMP (A,D,G,L) and in magenta for Ng (B,E,H,M; merged images in C,F,I,N). O: Quantification of Ng-expressing cells in the sEPL-GL region during postnatal development (P0–P30). Error bars indicate SEM. P: OB at P5 stained in magenta for Ng. Arrows indicate Ng-positive mitral cells. Q: Higher magnification image of a Ng-positive tufted cell at P15. Arrow indicates a basal dendrite oriented toward the EPL. GL, glomerular layer; sEPL, superficial external plexiform layer; MCL, mitral cell layer; GCL, granule cell layer. Scale bars = 25 μm in N (applies to A–M); 50 μm in P; 20 μm in Q.

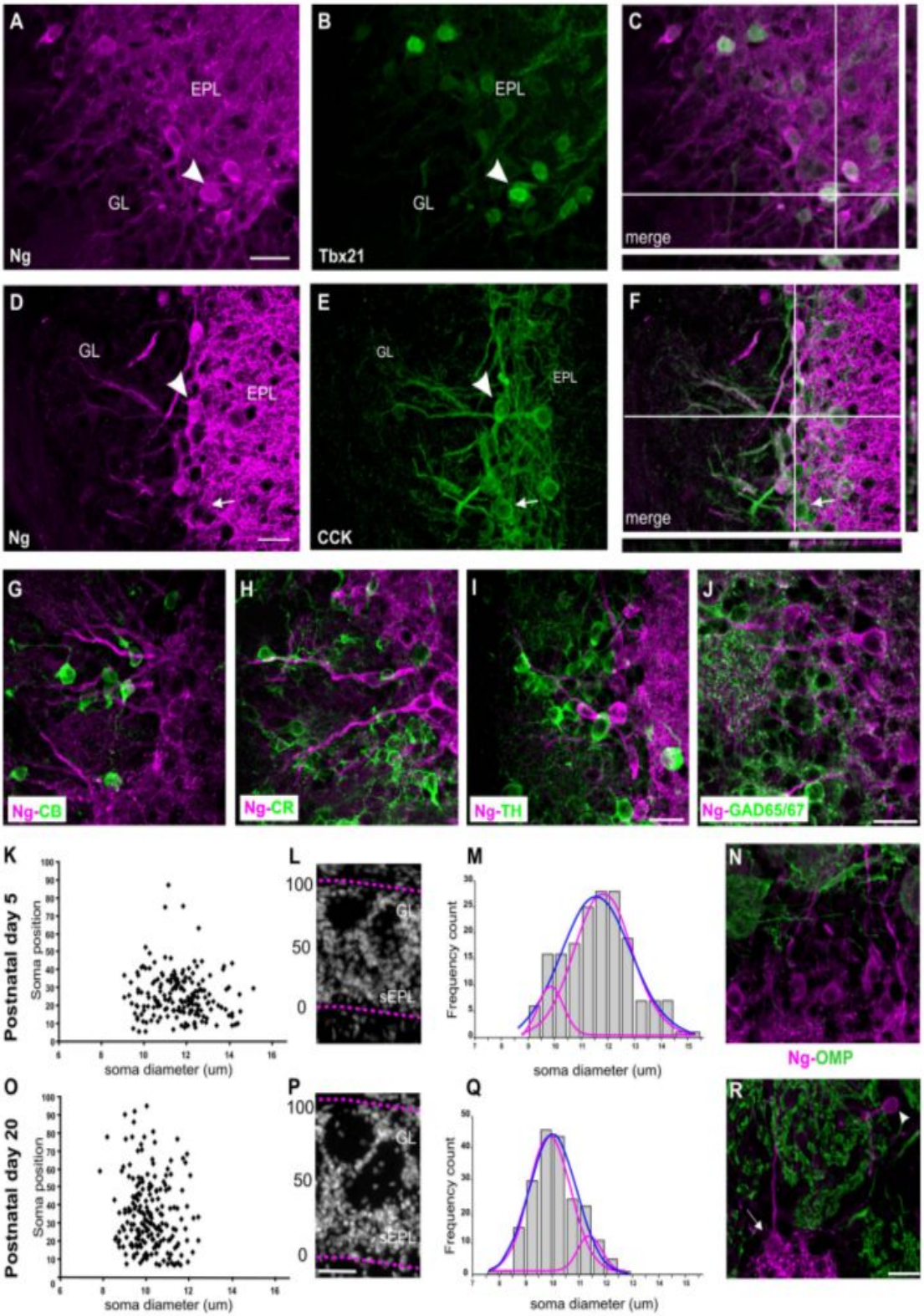

Figure 2. Neurochemical and morphometric characterization of Ng-positive cells in the sEPL-GL region of the developing OB. A–C: Confocal images of the sEPL-GL region stained in magenta for Ng (A) and in green for Tbx21 (B). The two proteins show a high level of coexpression (merged in C, single confocal plane). Arrowhead indicates a double-labeled cell. D–F: Confocal images of P10 sEPL-GL area stained in magenta for Ng (D) and in green for CCK (E). The two proteins show a high level of coexpression (merged in F, single confocal plane). Arrowhead indicates a double-labeled cell; arrow indicates a CCK-positive and Ng-negative cell. G–J: Confocal images of P10 (G,H,J) and P15 (I) sEPL-GL area stained in magenta for Ng and in green for CB (G), CR (H), TH (I), and GAD65/67 (J). K–R: Distribution of Ng-positive cell soma diameter and distance calculated from the lower border of the sEPL-GL region at P5 (K) and P20 (O). The thickness of the sEPL-GL region at different postnatal ages was normalized to 100 (L,P). The distribution of the soma diameter described by a single Gaussian curve is shown in blue (M at P5 and Q at P20),

whereas the soma diameter distribution fitting with two Gaussian curves is shown in magenta (M at P5 and Q at P20). Images of Ng-expressing cells (stained in magenta) at P5 (N) and P20 (R; arrow indicates a cell in the sEPL; arrowhead indicates a cell in the GL) showing different soma location in the sEPL-GL. OMP, green in N,R. GL, glomerular layer; sEPL, superficial external plexiform layer. Scale bars = 20 μm in A (applies to B–C); 20 μm in D (applies to E–F); 20 μm in I (applies to G–H); 20 lm in J; 50 lm in P (applies to L); 20 μm in R (applies to N).

acid decarboxylase, confirming that Ng-expressing cells in the sEPL-GL region are not GABAergic interneurons.

Tufted cells can be classified according to their cell body position and dimension as internal, middle, superficial, or external (Pinching and Powell, 1971; Macrides and Schneider, 1982; Orona et al., 1984). Analysis of Ng-positive cells in the sEPL-GL region indicates that both parameters vary significantly among ages (univariate ANOVA, soma size comparison P5, P10, P15, P20 $P < 0.001$, $F = 83.585$; position: $P < 0.001$, $F = 17.291$). To illustrate these variations, we plotted Ng-positive cell soma diameter and position (see Material and Methods for details) at P5 and P20 (Fig. 2K,O), when comparable density of Ng-positive cells is found in the sEPL-GL region (P5 238 ± 27, P20 224 ± 17 cells/mm 2 , mean ± SEM; n = 3). At P5, Ng is expressed by cells located mostly in the lower half of the sEPL-GL region (25.8 ± 0.9 μm, mean distance from the sEPL-GL lower border ± SEM; Fig. 2K,L,N), with soma diameter ranging from 9.1 to 15.1 lm. At P20, Ng-expressing cells are smaller (soma diameter ranging from 7.8 to 12.8 μm) and more dispersed within the sEPL-GL (34.9 μm ± 1.5, mean distance from the sEPL-GL lower border ± SEM; Fig. 2O–R *t*-test, P5 vs. P20 $P < 0.001$). The distribution of the soma diameter described by a single Gaussian curve shows a peak at 11.59 μm and a full width at half-maximum (FWHW) of 3.14 μm ($R^2 = 0.89$) at P5 (Fig. 2M) and a peak at 10.03 μm ± FWHW of 2.08 μm ($R^2 = 0.93$) at P20 (Fig. 2Q), indicating a leftward shift in the curve from P5 to P20 and supporting the idea that different subsets of tufted cells express Ng at distinct developmental stages (*t*-test on soma diameters, P5 vs. P20 $P < 0.0001$). Notably, the soma size distribution is also well fitted by two Gaussian curves that peak at similar values at both ages (P5 9.82 ± 0.77 and 11.79 ± 2.06, $R^2 = 0.96$; P20 9.91 ± 1.39 and 11.43 ± 0.61, $R^2 = 0.99$, peak value ± FWHW) but show inverted amplitude between P5 and P20 (Fig. 2M,Q), suggesting a switch in the cell subtypes expressing Ng during development. At P5, Ng-positive cells can be ascribed mainly to superficial tufted cells (Pinching and Powell, 1971; Macrides and Schneider, 1982), whereas, at P20, most Ng-positive elements, characterized by smaller soma and widespread localization into the sEPL-GL, can be attributed to external tufted cells (Pinching and Powell, 1971; Kosaka and Kosaka, 2007).

Early olfactory deprivation increases Ng-positive tufted cells in the sEPL-GL

During development, mitral and tufted cell apical dendrite refinement and maturation are influenced by neuronal activity elicited by sensory stimulation (Brunjes, 1994; Leon, 1998; Tyler et al., 2007; Maher et al., 2009). To investigate whether Ng expression in tufted cells could be modulated by afferent sensory activity, we performed early (from P0 to P1) olfactory sensory deprivation by naris occlusion (Brunjes, 1994; Fig. 3A). According to previous reports (Cummings et al., 1997), 20 days after deprivation, the OB ipsilateral to the closed naris has a reduced size (nearly 20% smaller) compared with control OB (Fig. 3B). In addition, the GL area occupied by OMP-positive OSN axonal shafts (Margolis, 1982), which progressively increases during normal postnatal development (Fig. 3C), is reduced in P15 and P20 deprived animals (univariate ANOVA; age $F = 431.770$, $P < 0.001$; deprivation $F = 63.617$, $P < 0.001$; age x deprivation $F = 24.106$, $P < 0.001$; P15 16%, *t*-test, $P < 0.01$; P20 27%, *t*-test, $P < 0.001$; Fig. 3C). Similarly, MAP-2 labeling of the glomeruli dendritic compartment shows a reduction in deprived animals (P20: 3,344.6 ± 174 vs. 2,435.4 ± 135.6 μm^2 ± SEM, standard vs. deprived, 27% reduction, *t*-test, $P < 0.001$). We therefore analyzed Ng expression at different survival time after naris occlusion (5, 10, 15, and 20 days; Fig. 3A). Only OBs showing a net decrease in TH immunofluorescence (indicative of effective deprivation; Baker et al., 1993) in the GL of deprived animals (Fig. 3H) were considered for the analysis. Olfactory deprivation significantly modifies the amount of Ng-positive cells in the sEPL-GL (Fig. 3D; univariate

ANOVA, age F = 47.567, P < 0.001; deprivation F = 18.398, P < 0.001; age x deprivation F = 5.264, P < 0.001). A net increase (40–115% increase) in the absolute number of Ng-expressing cells in deprived compared with standard condition was observed at P10, P15, and P20 (Fig. 3D). In parallel, we found an intensification of Ng immunostaining in the glomerular neuropil (Fig. 3I,J). As for standard mice, the expression of Ng in the sEPL-GL region of deprived mice virtually disappears by P30 (Fig. 3D), indicating that naris occlusion does not alter the temporal expression

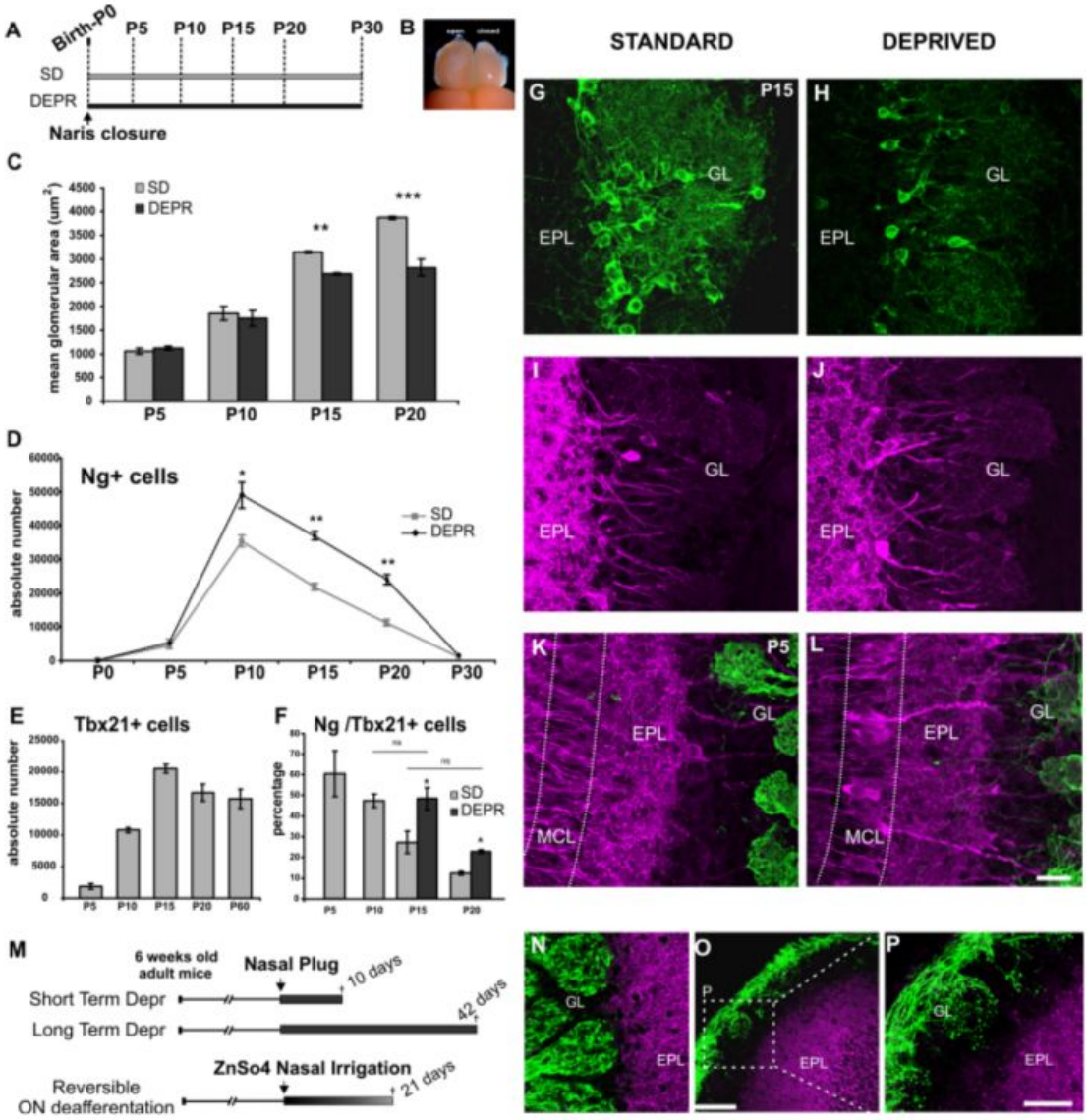

Figure 3. Early olfactory deprivation modulates Ng expression in the sEPL-GL region. A: Experimental protocol for early olfactory deprivation. B: Image showing P20 OBs following early olfactory deprivation. The OB ipsilateral to the closed naris is reduced compared with controlateral OB. C: Graph showing the OB mean glomerular area of mice maintained in deprived (DEPR) vs. standard (SD) condition. Error bars indicate SEM. **P < 0.01, ***P < 0.001. D: Estimate of absolute number of Ng-positive cells in the sEPL-GL region at different post-natal ages in DEPR vs. SD animals. Error bars indicate SEM; *P < 0.05, **P < 0.01. E,F: Estimate of Tbx21-expressing cells in sEPL-GL region at different postnatal ages (E) and percentage of Ng-positive cells expressing Tbx21 in DEPR vs. SD condition (F). Error bars indicate SEM. *P < 0.05; ns, not statistically significant. G–J: Confocal images of P15 sEPL-GL stained in green for TH (G,H) and in magenta for Ng (I,J) under standard (G,I) and deprived (H,J) conditions. K,L: Confocal images of P5 OB stained in magenta for Ng and in green for OMP under standard (K) and deprived (L) conditions. Dotted lines define the MCL. M: Experimental protocols used for olfactory deprivation in adults. N–P: Confocal images of adult OB stained in magenta for Ng and in green for OMP under standard condition (N) and 3 weeks following zinc sulfate nasal irrigation (O). P shows a higher magnification of the boxed area in O. GL, glomerular layer; EPL, external plexiform layer; MCL, mitral cell layer. Scale bars = 25 μm in L (applies to G–K); 100 μm in O; 50 μm in P (applies to N).

pattern of Ng in this region. The number of Ng-positive cells found at P15 and P20 under deprived conditions is comparable to that found under standard conditions at P10 and P15, respectively (Fig. 3D). Increased Ng-positive elements at these ages could result, at least in part, from a delay in Ng downregulation in tufted cells. To address this possibility, we analyzed the coexpression of Ng and Tbx21 in the sEPL-GL region (Fig. 3E,F). Indeed, Tbx21 expression settles on stable levels from P15–P20 (Fig. 3E) and does not change following olfactory deprivation (P15 20,705 ± 611 vs. 20,802 ± 4,071 standard vs. deprived, absolute number of cells ± SEM, *t*-test, P = 0.9823). Under standard conditions, the number of Ng-positive cells double labeled for Tbx21 progressively decrease from P5 to P20 (Fig. 3F). On the other hand, the percentage of double-labeled cells is significantly increased in deprived animals at P15 and P20, reaching values not significantly different from those observed at P10 and P15, respectively, under control conditions (Fig. 3F), supporting a delay in Ng downregulation in Tbx21-positive cells.
Notably, after short-term deprivation (from P0 to P5), a strong Ng immunostaining appears in cell bodies and apical processes of mitral cells (Fig. 3K,L) that, under standard conditions, show no or weak labeling for Ng (Fig. 1P). No labeling in mitral cells is observed at longer survival times under either standard or deprived conditions. In the GCL, sensory deprivation does not induce any change in the number of Ng-positive GCs compared with standard conditions (absolute number of cells ± SEM at P15 39,650 ± 2,225 vs. 48,149 ± 2,092, *t*-test, P = 0.109).

Activity-dependent modulation of Ng expression in tufted cells is a peculiar feature of developmental stages

In adults, Ng expression is virtually absent in OB projection neurons, and only rare Ng-positive cells can be detected in the sEPL-GL region (Gribaudo et al., 2009). We asked whether Ng expression in these neurons could be reactivated by manipulation of the olfactory input in adults. With this aim, we performed short (10 days)- and long (42 days)-term naris closure to interfere with olfactory experience (Fig. 3M). Our results show that both short- and long-term olfactory deprivation protocols do not induce any change in Ng expression in sEPL-GL region. Additionally, we performed a chemical lesion of the olfactory epithelium by ZnSO 4 nasal irrigation, which leads to rapid depletion of OSNs, inducing drastic changes in the glomerular circuit organization (Burd, 1993; Ducray et al., 2002), and analyzed Ng expression 3 weeks later (Fig. 3M). In ZnSO 4 -treated mice, sparse OMP-positive fibres were observed in the GL (Fig. 3N–P), suggesting a partial reinnervation of the glomeruli by newborn OSNs (Williams et al., 2004). Also in this case, no Ng-positive tufted cells were detected in treated mice (Fig. 3N–P). Similarly, no Ng immunostaining was observed in mature mitral cells following any of the olfactory deprivation paradigms, indicating that sensory modulation of Ng expression in OB projection neurons is a peculiar feature of developmental stages.

DISCUSSION

This study characterizes Ng expression in the OB during postnatal development. We showed that, in addition to GCs, which express Ng throughout life (Gribaudo et al., 2009), a strong labeling for Ng transiently occurs in subsets of tufted cells in the sEPL-GL region from P5 to P20. Two main tufted cell subtypes, the superficial and external tufted cells, classified based on their laminar position, soma size, and secondary dendrite extension (Pinching and Powell, 1971; Macrides and Schneider 1982; Hayar et al., 2004), are located in the sEPL-GL region. Both cell subtypes retain the classic apical dendrite that branches, forming a tuft within a single glomerulus (Pinching and Powell, 1971; Macrides and Schneider, 1982), but, whereas superficial tufted cells are larger and located in the deep GL or sEPL, external tufted cells are distributed predominantly in the superficial two-thirds of the GL (Pinching and Powell, 1971; Schneider and Macrides, 1978; Orona et al., 1984; Antal et al., 2006). Based on morphological criteria, our findings indicate that, at P5, most Ng-positive cells are superficial tufted cells, whereas, at P20, most Ng-positive elements belong to the external tufted cell population (Macrides and Schneider, 1982; Kosaka and Kosaka, 2007). Although there is

considerable overlap in the temporal pattern of generation of different tufted cell subtypes during embryonic development, an inside-out pattern has been described, with deeper cells originating at early embryonic stages and external tufted cells the last to be produced at later embryonic and perinatal stages (Hinds, 1968; Winpenny et al., 2011). Thus, the sequential appearance of Ng-positive superficial and external tufted cells could correlate with the successive generation and maturation of the two subtypes.

We showed that the number of Ng-positive tufted cells peaks at P10, progressively decreases at P15 and P20, to reach the adult-like condition (none or rare positive elements) by P30. This time course correlates with the sensitive phase described for mitral/tufted cell maturation, involving extensive dendritic growth, remodelling and pruning, and increase in synaptic density (Hinds and Hinds, 1976; Imamura and Greer, 2009; Marcucci et al., 2011). Accordingly, in the GL, Ng-positive processes increase in extent and intensity during the first 2 post-natal weeks along with glomerular enlargement. At P20, when tufted cell apical dendritic tufts are likely to be matured and less dynamic (Mizrahi and Katz, 2003; Blanchart et al., 2006; Imamura and Greer, 2009), no more Ng labeling is found in the glomeruli. Thus, the time span of Ng expression in superficial/external tufted cells could reflect its involvement in the formation and stabilization of the dendritic arbor and synaptogenesis in the OB glomeruli, as previously suggested for other telencephalic regions (Alvarez-Bolado et al., 1996). Future studies, using Ng knockout mice (Pak et al., 2000), should be undertaken to investigate further the role of Ng in OB development and function. Indeed, adult Ng knockout mice have been previously demonstrated to exhibit severe deficits in hippocampus-dependent spatial learning (Pak et al., 2000; Wu et al., 2002; Huang et al., 2004), but no data are available on possible developmental defects and/or deficits in olfactory-related functions.

The physiological maturation of glomerular circuits is influenced by sensory activity (Frazier and Brunjes, 1988; Royet et al., 1989; Brunjes, 1994; Matsutani and Yamamoto, 2000; Lin et al., 2000; Belluscio et al., 2002; Nakatani et al., 2003; Maher et al., 2009). In particular, post-natal naris closure has been shown to delay mitral cellapical dendrite maturation and alter tufted cell connections (Meisami and Noushinfar, 1986; Matsutani and Yamamoto, 2000; Marks et al., 2006). Although conflicting results have been reported (Meisami and Safari, 1981; Benson et al., 1984; Frazier and Brunjes, 1988; Fiske and Brunjes, 2001), the number of mitral and tufted cells does not seem to be greatly affected by naris closure. We showed that early olfactory deprivation reduces glomerular neuropil extension, supporting an alteration in glomerular circuit development, according to previous reports (Meisami and Safari, 1981; Meisami and Noushinfar, 1986; Frazier and Brunjes, 1988; Matsutani and Yamamoto, 2000; Couper Leo et al., 2000; Marks et al., 2006). We demonstrated that early naris closure induces a significant increase in the number of tufted cells expressing Ng. This effect is confined within the developmental time window for Ng expression under physiological conditions (P5–P20). Naris occlusion could induce Ng expression in tufted cells that do not normally express Ng at detectable levels and/or extend the duration of Ng expression by anticipating its onset or by delaying its downregulation. Although we cannot exclude an ex novo expression of Ng in tufted cells, our data support the idea that the increase in the positive cell number under deprived conditions reflects a delay in Ng physiological downregulation. Indeed, in deprived animals, at P15 and P20, both the absolute number of Ng-expressing cells and the percentage of Ng cells double-labeled for Tbx21 show values comparable to those at P10 and P15 under standard conditions, respectively. The differences observed in the absolute numbers of Ng-positive cells at P10 in deprived vs. standard OBs may be due to a persistence of Ng expression in early generated superficial tufted cells that would have normally switched off Ng expression at this stage. On the other hand, Ng expression following olfactory deprivation in mitral cells at P5 likely is due to an upregulation of the protein and is possibly related to the mitral cell critical maturational phase (Matsutani and Yamamoto, 2000; Blanchart et al., 2006; Imamura and Greer, 2009), which closes earlier compared with tufted cells. Accordingly, the effects described from previous studies on mitral cell dendrite differentiation following early naris closure were confined between P1 and P10 (Matsutani and Yamamoto, 2000). Contrary to early post-natal deprivation,

olfactory manipulation in adult mice does not induce expression of Ng in tufted or mitral cells, suggesting a role for Ng in the establishment/maturation of mitral and tufted cell dendrites and synaptic contacts rather than in the maintenance of their stability. Indeed, neither the block of incoming stimuli obtained by naris closure nor OSN chemical deafferentation alters Ng expression in these cells. Accordingly, sensory deprivation in adult mice does not induce morphological alteration of OB mature projection neurons, which in adults maintain a high degree of structural stability (Matsutani and Yamamoto, 2000; Mizrahi and Katz, 2003).

Previous studies showed that early olfactory deprivation increases the responsiveness of mitral/tufted cells (Tyler et al., 2007; Aylwin et al., 2009). This involves a decrease in the glomerular feedback inhibition (Wilson and Sullivan, 1995), changes at the dendrodendritic synapses between GCs and mitral/tufted cells (Saghatelyan et al., 2005), and pre- and postsynaptic changes at primary olfactory synapses dependent mainly on Ca^{2+} and Ca^{2+} -sensitive molecules (Tyler et al., 2007). Ng is a molecular mediator that enhances the Ca^{2+} -dependent transduction signalling by reinforcing CaM concentration at postsynaptic sites in a critical cell developmental time window (Gerendasy and Sutcliffe, 1997). Ng mRNA is dendritically targeted through its 3'-untranslated region, and its local translation could be concurrent with rapid changes in Ng protein expression at synapses (Mori et al., 2000; Pinkstaff et al., 2001; Gao et al., 2008). In this scenario, Ng regulation following early olfactory deprivation could be part of a compensatory response, occurring at the postsynaptic sites of primary olfactory synapses, directed to enhance cell sensitivity in response to decreased incoming stimuli during activity-dependent circuit maturation.

ACKNOWLEDGMENTS

We thank S. Geuna for advice on morphometric methods, O. Belluzzi and A. Pignatelli for help with data analysis, and P. Peretto for helpful discussion and critical reading of the manuscript.

LITERATURE CITED

Allen ZJ, Waclaw RR, Colbert MC, Campbell K. 2007. Molecular identity of olfactory bulb interneurons: transcriptional codes of periglomerular neuron subtypes. J Mol Histol 38: 517–525.

Alvarez-Bolado G, Rodriguez-Sanchez P, Tejero-Diez P, Fairen A, Diez-Guerra FJ. 1996. Neurogranin in the development of the rat telencephalon. Neuroscience 73:565–580.

Antal M, Eyre M, Finklea B, Nusser Z. 2006. External tufted cells in the main olfactory bulb form two distinct subpopulations. Eur J Neurosci 24:1124–1136.

Aylwin ML, Aguilar GA, Flores FJ, Maldonado PE. 2009. Odorant modulation of neuronal activity and local field potential in sensory-deprived olfactory bulb. Neuroscience 162: 1265–1278.

Baker H, Grillo M, Margolis FL. 1989. Biochemical and immunocytochemical characterization of olfactory marker protein in the rodent central nervous system. J Comp Neurol 285:246–261.

Baker H, Morel K, Stone DM, Maruniak JA. 1993. Adult naris closure profoundly reduces tyrosine hydroxylase expression in mouse olfactory bulb. Brain Res 614:109–116.

Belluscio L, Lodovichi C, Feinstein P, Mombaerts P, Katz LC. 2002. Odorant receptors instruct functional circuitry in the mouse olfactory bulb. Nature 419:296–300.

Benson TE, Ryugo DK, Hinds JW. 1984. Effects of sensory deprivation on the developing mouse olfactory system: a light and electron microscopic, morphometric analysis. J Neurosci 4:638–653.

Blanchart A, De Carlos JA, Lopez-Mascaraque L. 2006. Time frame of mitral cell development in the mice olfactory bulb. J Comp Neurol 496:529–543.

Blanchart A, Romaguera M, Garcı´a-Verdugo JM, de Carlos JA, Lopez-Mascaraque L. 2008. Synaptogenesis in the mouse olfactory bulb during glomerulus development. Eur J Neurosci 27:2838–2846.

Blue ME, Parnavelas JG. 1983. The formation and maturation of synapses in the visual cortex of the rat. I. Qualitative analysis. J Neurocytol 12:599–616.

Brunjes PC. 1994. Unilateral naris closure and olfactory system development. Brain Res Brain Res Rev 19:146–160.
Burd GD. 1993. Morphological study of the effects of intranasal zinc sulfate irrigation on the mouse olfactory epithelium and olfactory bulb. Microsc Res Techniq 24:195–213.
Chakravarthy B, Morley P, Whitfield J. 1999. Ca^{2+} -calmodulin and protein kinase Cs: a hypothetical synthesis of their conflicting convergences on shared substrate domains. Trends Neurosci 22:12–16.
Ciofi P, Tramu G. 1990. Distribution of cholecystokinin-like-immunoreactive neurons in the guinea pig forebrain. J Comp Neurol 300:82–112.
Couper Leo JM, Devine AH, Brunjes PC. 2000. Focal denervation alters cellular phenotypes and survival in the rat olfactory bulb: a developmental analysis. J Comp Neurol 425: 409–421.
Cummings DM, Henning HE, Brunjes PC. 1997. Olfactory bulb recovery after early sensory deprivation. J Neurosci 17: 7433–7440.
Ducray A, Bondier JR, Michel G, Bon K, Millot JL, Propper A, Kastner A. 2002. Recovery following peripheral destruction of olfactory neurons in young and adult mice. Eur J Neurosci 15:1907–1917.
Dotti CG, Banker GA, Binder LI. 1987. The expression and distribution of the microtubule-associated protein tau and microtubule-associated protein 2 in hippocampal neurons in the rat in situ and in cell culture. Neuroscience 23: 121–130.
Ennis M, Hamilton KA, Hayar A. 2007. Neurochemistry of the main olfactory system. In: Johnson DA, editor. Handbook of neurochemistry and molecular neurobiology. Heidelberg: Springer. p 137–204.
Faedo A, Ficara F, Ghiani M, Aiuti A, Rubenstein JL, Bulfone A. 2002. Developmental expression of the T-box transcription factor T-bet/Tbx21 during mouse embryogenesis. Mech Dev 116:157–160.
Fiske BK, Brunjes PC. 2001. Cell death in the developing and sensory-deprived rat olfactory bulb. J Comp Neurol 431: 311–319.
Frazier LL, Brunjes PC. 1988. Unilateral odor deprivation: early postnatal changes in olfactory bulb cell density and number. J Comp Neurol 269:355–370.
Gao Y, Tatavarty V, Korza G, Levin MK, Carson JH. 2008. Multiplexed dendritic tergeting of alpha calcium calmodulin-dependent protein kinase II, neurogranin, and activityregulated cytoskeleton-associated protein RNAs by the A2 pathway. Mol Biol Cell 5:2311–2327.
Gerendasy D. 1999. Homeostatic tuning of Ca^{2+} signal transduction by members of the calpacitin protein family. J Neurosci Res 58:107–119.
Gerendasy DD, Sutcliffe JG. 1997. RC3/neurogranin, a postsynaptic calpacitin for setting the response threshold to calcium influxes. Mol Neurobiol 15:131–163.
Giachino C, De Marchis, Giampietro C, Parlato R, Perroteau I, Schutz G, Fasolo A, Peretto P. 2005. cAMP response element-binding protein regulates differentiation and survival of newborn neurons in the olfactory bulb. J Neurosci 25:
10105–10118.
Gribaudo S, Bovetti S, Garzotto D, Fasolo A, De Marchis. 2009. Expression and localization of the calmodulin-binding protein neurogranin in the adult mouse olfactory bulb. J Comp Neurol 517:683–694.
Hayar A, Karnup S, Shipley MT, Ennis M. 2004. Olfactory bulb glomeruli: external tufted cells intrinsically burst at theta frequency and are entrained by patterned olfactory input. J Neurosci 24:1190–1199.
Higo N, Oishi T, Yamashita A, Murata Y, Matsuda K, Hayashi M. 2006. Expression of protein kinase C-substrate mRNAs in the basal ganglia of adult and infant macaque monkeys. J Comp Neurol 499:662–676.
Hinds JW. 1968. Autoradiographic study of histogenesis in the mouse olfactory bulb. I. Time of origin of neurons and neuroglia. J Comp Neurol 134:287–304.

Hinds JW, Hinds PL. 1976. Synapse formation in the mouse olfactory bulb. II. Morphogenesis. J Comp Neurol 169: 41–61.
Huang KP, Huang FL, Jäger T, Li J, Reymann KG, Balschun D. 2004. Neurogranin/RC3 enhances long-term potentiation and learning by promoting calcium-mediated signaling. J Neurosci 24:10660–10669.
Imamura F, Greer CA. 2009. Dendritic branching of olfactory bulb mitral and tufted cells: regulation by TrkB. PLoS ONE 4:e6729.
Kasowski HJ, Kim H, Greer CA. 1999. Compartmental organization of the olfactory bulb glomerulus J Comp Neurol 407:261–274.
Kondo K, Suzukawa K, Sakamoto T, Watanabe K, Kanaya K, Ushio M, Yamaguchi T, Nibu K, Kaga K, Yamasoba T. 2010. Age-related changes in cell dynamics of the postnatal mouse olfactory neuroepithelium: cell proliferation, neuronal differentiation, and cell death. J Comp Neurol 518:1962–1975.
Kosaka K, Kosaka T. 2007. Chemical properties of type 1 and type 2 periglomerular cells in the mouse olfactory bulb are different from those in the rat olfactory bulb. Brain Res1167:42–55.
Kubota Y, Putkey JA, Waxham MN. 2007. Neurogranin controls the spatiotemporal pattern of postsynaptic Ca^{2+}/CaM signaling. Biophys J 93:3848–3859.
Larouche M, Che PM, Hawkes R. 2006. Neurogranin expression identifies a novel array of Purkinje cell parasagittal stripes during mouse cerebellar development. J Comp Neurol 494:215–227.
Leon M. 1998. Compensatory responses to early olfactory restriction. Ann N Y Acad Sci 855:104–108.
Lin DM, Wang F, Lowe G, Gold GH, Axel R, Ngai J, Brunet L. 2000. Formation of precise connections in the olfactory bulb occurs in the absence of odorant-evoked neuronal activity. Neuron 26:69–80.
Liu WL, Shipley MT. 1994. Intrabulbar associational system in the rat olfactory bulb comprises cholecystokinin-containing tufted cells that synapse onto the dendrites of GABAergic granule cells. J Comp Neurol 346:541–558.
Macrides F, Schneider SP. 1982. Laminar organization of mitral and tufted cells in the main olfactory bulb of the adult hamster. J Comp Neurol 208:419–430.
Maher BJ, McGinley MJ, Westbrook GL. 2009. Experience-dependent maturation of the glomerular microcircuit. Proc Natl Acad Sci U S A 106:16865–16870.
Marcucci F, Maier-Balough E, Zou DJ, Firestein S. 2011. Exuberant growth and synapse formation of olfactory sensory neuron axonal arborizations. J Comp Neurol 519:
3713–3726.
Margolis FL. 1982. Olfactory marker protein (OMP). Scand J Immunol Suppl 9:181–199.
Marks CA, Cheng K, Cummings DM, Belluscio L. 2006. Activity-dependent plasticity in the olfactory intrabulbar map. J Neurosci 26:11257–11266.
Matsutani S, Yamamoto N. 2000. Differentiation of mitral cell dendrites in the developing main olfactory bulbs of normal and naris-occluded rats. J Comp Neurol 418:402–410.
Meisami E, Noushinfar E. 1986. Early olfactory deprivation and the mitral cells of the olfactory bulb: a Golgi study. Int J Dev Neurosci 4:431–444.
Meisami E, Safari L. 1981. A quantitative study of the effects of early unilateral olfactory deprivation on the number and distribution of mitral and tufted cells and of glomeruli in the rat olfactory bulb. Brain Res 221:81–107.
Meisami E, Louie J, Hudson R, Distel H. 1990. A morphometric comparison of the olfactory epithelium of newborn and weanling rabbits. Cell Tissue Res 262:89–97.
Mizrahi A, Katz LC. 2003. Dendritic stability in the adult olfactory bulb. Nat Neurosci 6:1201–1207.
Mitsui S, Igarashi KM, Mori K, Yoshihara Y. 2011. Genetic visualization of the secondary olfactory pathway in Tbx21 transgenic mice. Neural Syst Circuits 1:5.
Mori Y, Imaizumi K, Katayama T, Yoneda T, Tohyama M. 2000. Two cis-acting elements in the 3'

untranslated region of alpha-CaMKII regulate its dendritic targeting. Nat Neurosci 3:1079–1084.
Nakatani H, Serizawa S, Nakajima M, Imai T, Sakano H. 2003. Developmental elimination of ectopic projection sites for the transgenic OR gene that has lost zone specificity in the olfactory epithelium. Eur J Neurosci 18:2425–2432.
Orona E, Rainer EC, Scott JW. 1984. Dendritic and axonal organization of mitral and tufted cells in the rat olfactory bulb. J Comp Neurol 226:346–356.
Pak JH, Huang FL, Li J, Balschun D, Reymann KG, Chiang C, Westphal H, Huang KP. 2000. Involvement of neurogranin in the modulation of calcium/calmodulin-dependent protein kinase II, synaptic plasticity, and spatial learning: a study with knockout mice. Proc Natl Acad Sci U S A 97: 11232–11237.
Pinching AJ, Powell TP. 1971. The neuron types of the glomerular layer of the olfactory bulb. J Cell Sci 9:305–345.
Pinkstaff JK, Chappell SA, Mauro VP, Edelman GM, Krushel LA. 2001. Internal initiation of translation of five dendritically localized neuronal mRNAs. Proc Natl Acad Sci USA 98:2770–2775.
Porteous R, Petersen SL, Yeo SH, Bhattarai JP, Ciofi P, Colledge WH, Caraty A, Herbison AE. 2011. Kisspeptin neurons co-express met-enkephalin and galanin in the rostral periventricular region of the female mouse hypothalamus. J Comp Neurol 519:3456–3469.
Represa A, Deloulme JC, Sensenbrenner M, Ben-Ari Y, Baudier J. 1990. Neurogranin: immunocytochemical localization of a brain-specific protein kinase C substrate. J Neurosci 10: 3782–3792.
Reyes BAS, Johnson AD, Glaser JD, Commons KG, Van Bockstaele EJ. 2007. Dynorphin-containing axons directly innervate noradrenergic neurons in the rat nucleus locus coeruleus. Neuroscience 145:1077–1086.
Royet JP, Jourdan F, Ploye H. 1989. Morphometric modifications associated with early sensory experience in the rat olfactory bulb: I. Volumetric study of the bulbar layers. J Comp Neurol 289:586–593.
Saghatelyan A, Roux P, Migliore M, Rochefort C, Desmaisons D, Charneau P, Shepherd GM, Lledo PM. 2005. Activity-dependent adjustments of the inhibitory network in the olfactory bulb following early postnatal deprivation. Neuron 46: 103–116.
Schneider SP, Macrides F. 1978. Laminar distributions of internuerons in the main olfactory bulb of the adult hamster. Brain Res Bull 3:73–82.
Schwob JE, Szumowski KE, Stasky AA. 1992. Olfactory sensory neurons are trophically dependent on the olfactory bulb for their prolonged survival. J Neurosci 12: 3896–3919.
Singec I, Knoth R, Ditter M, Volk B, Frotscher M. 2004. Neurogranin is expressed by principal cells but not interneurons in the rodent and monkey neocortex and hippocampus. J Comp Neurol 479:30–42.
Steward O, Falk PM. 1991. Selective localization of polyribosomes beneath developing synapses: a quantitative analysis of the relationships between polyribosomes and developing synapses in the hippocampus and dentate gyrus. J Comp Neurol 314:545–557.
Studler JM, Reibaud M, Tramu G, Blanc G, Glowinski J, Tassin JP. 1984. Pharmacological study on the mixed CCK8/DA meso-nucleus accumbens pathway: evidence for the existence of storage sites containing the two transmitters. Brain Res 298:91–97.
Treloar HB, Purcell AL, Greer CA. 1999. Glomerular formation in the developing rat olfactory bulb. J Comp Neurol 413: 289–304.
Tyler WJ, Petzold GC, Pal SK, Murthy VN. 2007. Experience-dependent modification of primary sensory synapses in the mammalian olfactory bulb. J Neurosci 27:9427–9438.
Van Bockstaele EJ, Pickel VM. 1993. Ultrastructure of serotoninimmunoreactive terminals in the core and shell of the rat nucleus accumbens: cellular substrates for interactions with catecholamine afferents. J Comp Neurol 334: 603–617.

van Dalen JJ, Gerendasy DD, de Graan PN, Schrama LH, Gruol DL. 2003. Calcium dynamics are altered in cortical neurons lacking the calmodulin-binding protein RC3. Eur J Neurosci 18:13–22.
Verhaagen J, Oestreicher AB, Gispen WH, Margolis FL. 1989. The expression of the growth associated protein B50/GAP43 in the olfactory system of neonatal and adult rats.J Neurosci 9:683–691.
Whitman MC, Greer CA. 2007. Adult-generated neurons exhibit diverse developmental fates. Dev Neurobiol 67: 1079–1093.
Wichterle H, Turnbull DH, Nery S, Fishell G, Alvarez-Buylla A. 2001. In utero fate mapping reveals distinct migratory pathways and fates of neurons born in the mammalian basal forebrain. Development 128:3759–3771.
Williams SK, Gilbey T, Barnett SC. 2004. Immunohistochemical studies of the cellular changes in the peripheral olfactory system after zinc sulfate nasal irrigation. Neurochem Res 29:891–901.
Wilson DA, Sullivan RM. 1995. The D2 antagonist spiperone mimics the effects of olfactory deprivation on mitral/tufted cell odor response patterns. J Neurosci 15:5574–5581.
Winpenny E, Lebel-Potter M, Fernandez ME, Brill MS, G€ otz M, Guillemot F, Raineteau O. 2011. Sequential generation of olfactory bulb glutamatergic neurons by Neurog2-expressing precursor cells. Neural Dev 6:12.
Wu J, Li J, Huang KP, Huang FL. 2002. Attenuation of protein kinase C and cAMP-dependent protein kinase signal transduction in the neurogranin knockout mouse. J Biol Chem 277:19498–19505.
Wu J, Huang KP, Huang FL. 2003. Participation of NMDA-mediated phosphorylation and oxidation of neurogranin in the regulation of Ca^{2+} - and Ca^{2+} /calmodulin-dependent neuronal signaling in the hippocampus. J Neurochem 86: 1524–1533.
Yamamoto T, Yamato E, Tashiro F, Sato T, Noso S, Ikegami H, Tamura S, Yanagawa Y, Miyazaki JI. 2004. Development of autoimmune diabetes in glutamic acid decarboxylase 65 (GAD65) knockout NOD mice. Diabetologia 47:221–224.
Yoshihara S, Omichi K, Yanazawa M, Kitamura K, Yoshihara Y. 2005. Arx homeobox gene is essential for development of mouse olfactory system. Development 132:751–762.
Zhabotinsky AM, Camp RN, Epstein IR, Lisman JE. 2006. Role of the neurogranin concentrated in spines in the induction of long-term potentiation. J Neurosci 26:7337–7347.
Zhong L, Cherry T, Bies CE, Florence MA, Gerges NZ. 2009. Neurogranin enhances synaptic strength through its interaction with calmodulin. EMBO J 28:3027–3039.
Zhong L, Kaleka KS, Gerges NZ. 2011. Neurogranin phosphorylation fine-tunes long-term potentiation. Eur J Neurosci
33:244–250.